Hydrodynamic interactions and membrane damage for a pair of microcapsules in shear flow: Effect of membrane mechanical properties

Xu-Qu Hu, Claire Dupont, Anne-Virginie Salsac, Dominique Barthès-Biesel

Graphical Abstract

Hydrodynamic interactions and membrane damage for a pair of microcapsules in shear flow: Effect of membrane mechanical properties

Xu-Qu Hu, Claire Dupont, Anne-Virginie Salsac, Dominique Barthès-Biesel

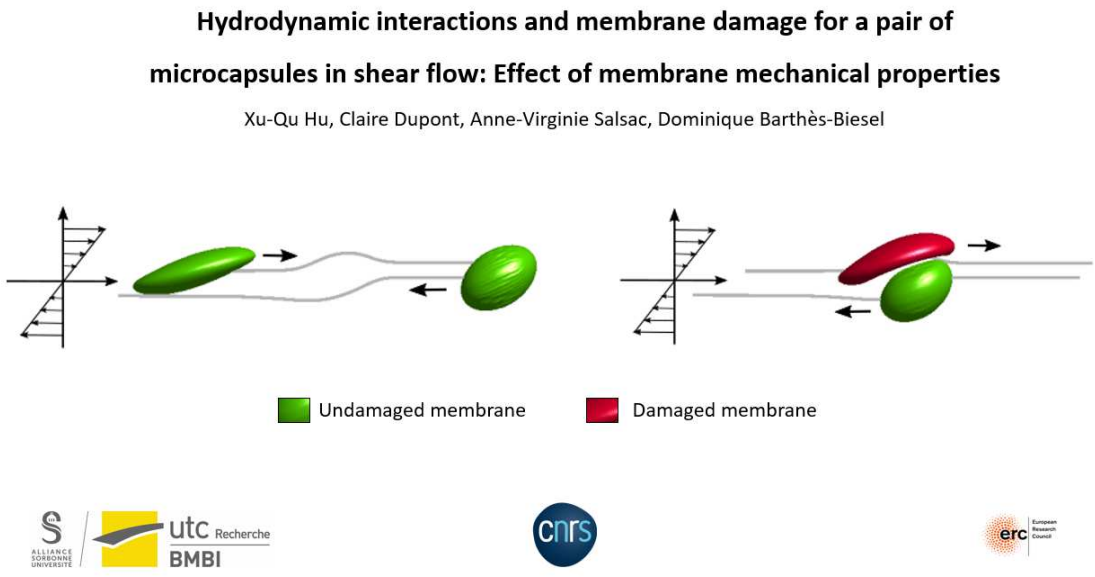

Highlights

Hydrodynamic interactions and membrane damage for a pair of microcapsules in shear flow: Effect of membrane mechanical properties

Xu-Qu Hu, Claire Dupont, Anne-Virginie Salsac, Dominique Barthès-Biesel

- Hydrodynamic interaction of two capsules with different mechanical properties
- Interaction induced damage to capsules

Hydrodynamic interactions and membrane damage for a pair of microcapsules in shear flow: Effect of membrane mechanical properties

Xu-Qu Hu, Claire Dupont, Anne-Virginie Salsac, Dominique Barthès-Biesel*

Biomechanics and Bioengineering Laboratory (UMR 7338), Université de Technologie de Compiègne - CNRS, 60203 Compiègne, France

Abstract

We model the hydrodynamic interaction of two equal size capsules in simple shear flow. The capsules may have different mechanical membrane properties. The results are analyzed in terms of a macro scale model of capsule membrane damage. We show how the interaction between two capsules with a membrane rigidity mismatch may lead to damage of the more deformable capsule even when the base flow strength is below the damage threshold of both capsules. We provide charts of the peak deformation energy density in the two membranes as a function of the flow strength and the ratio of the elastic rigidity of the two capsules. Given a damage criterion, those charts can be used to determine when flow-induced damage will occur in a suspension of capsules with a distribution of mechanical properties.

Keywords: capsule interaction, damage criterion, finite element method, boundary integral method

1. Introduction

Microcapsules, consisting of an internal medium enclosed in a thin elastic shell, are used for many industrial and medical applications to protect the internal cargo during transport until delivery. Their advantage, compared to lipid vesicles or liposomes, is that the polymerized membrane brings resistance to mechanical stresses even under fairly large deformation. Nevertheless a single capsule will eventually burst when it is subjected to an external stress that exceeds a critical value (Barthès-Biesel, 1991; Chang and Olbricht, 1993a,b; Walter et al., 2000; Rehage et al., 2002;

*The two first authors contributed equally. Corresponding author. E-mail: dbb@utc.fr

Carin et al., 2003; Risso and Carin, 2004; Koleva and Rehage, 2012; de Loubens et al., 2014; Ghaemi et al., 2016; Le Goff et al., 2017; Wang et al., 2021; Leopércio et al., 2021). Consequently, when capsules are suspended in a liquid carrier where they are subjected to hydrodynamic stresses, it is important to ensure that they are not damaged during transport. The base flow shear stress should thus be below the nominal limit of single capsule break-up.

But a complexity comes from the fact that capsule interactions modify the stress distribution. In semi-dilute suspensions, pair interactions between particles are the dominant effect (Guazzelli and Morris, 2012). The strongest interaction effects occur when the two capsules have their centers in the same shear plane on two nearby streamlines, corresponding to almost head on collision. In this situation, the two capsules are displaced along the velocity gradient direction and overpass each other: this is the so-called leap frog motion. At the peak of interaction, the shape distortion of the capsules goes through a maximum value before returning to its nominal value corresponding to the base flow deforming effect. After crossing, the separation between the capsule centers trajectories is larger than it was initially: it is this phenomenon which leads to self diffusion. Self diffusion effect has been extensively studied and is now well documented for two identical spherical elastic capsules suspended in a simple shear flow, and flowing in the same shear plane (Lac et al., 2007; Doddi and Bagchi, 2008), two vesicles (Kantsler et al., 2008; Gires et al., 2014) or two red blood cells (Omori et al., 2013). The self diffusion phenomenon has also been observed when the capsules flow in a polymeric liquid (Pranay et al., 2010). The case of two capsules with the same size but different membrane elastic properties has been considered by Singh and Sarkar (2015) who found that the trajectory shift was mildly influenced by the elastic moduli ratio. When two identical capsules are in different shear planes, the interaction and the trajectory shift decrease as the distance between the capsules increases (Lac and Barthès-Biesel, 2008; Gires et al., 2014). Furthermore, in this configuration, the two capsules may undergo a minuet motion where trajectory reversal and multiple interactions occur (Hu et al., 2020).

Most existing studies have characterized the mechanical state of the deformed capsule by means of an equivalent Taylor deformation parameter $D = (L_M - L_m)/(L_M + L_m)$ where L_M and L_m are the maximum and minimum lengths of the capsule deformed profile in the shear plane. The issue is that the capsule shapes during interaction are far from being ellipsoidal, which strongly limits the relevance of using such a deformation index. It is thus impossible to predict whether the capsule will be damaged by the interaction process from the value of D.

It is the purpose of this paper to analyze the stresses in the membrane of the capsule during pair interaction and verify if the extra transient deformation may

lead to damage of the membrane and ultimate loss of the enclosed material. In order to do so, we model the hydrodynamic interaction of two capsules with equal size but eventual differences in the mechanical membrane properties and analyze the results in terms of the recent macro scale model of capsule membrane damage in simple shear flow, developed by Grandmaison et al. (2021). This model is based on the theory of continuum damage mechanics: when the elastic energy density in the membrane exceeds a threshold value, damage in the membrane develops until break up occurs. We show how the interaction between two capsules with a membrane rigidity mismatch may lead to damage of the more deformable capsule even when the base flow strength is below the damage threshold of both capsules. We provide charts of the peak deformation energy density in the two membranes as a function of the flow strength and the ratio of the elastic rigidity of the two capsules. Given a damage criterion, those charts can be used to determine when flow induced damage will occur in the suspension of capsules. Consequently, those results can be used to determine safe flow conditions for a suspension of capsules or to sort capsules according to their membrane resistance.

In section 2, we present the hydrodynamic problem and the numerical method used to solve it. The dynamics of capsule crossing and the influence of the flow parameters are developed in section 3. The conditions for potential mechanical damage in one capsule membrane are analyzed in section 4. In section 5, we conclude and discuss how our results can be used in practice to either protect all the capsules or sort out the more deformable ones.

2. Problem statement and numerical method

2.1. Problem description

We consider two spherical capsules C_i ($i = 1, 2$) with identical radii a but potentially different mechanical properties. The capsule walls are assumed to be infinitely thin sheets of an incompressible isotropic neo-Hookean material. Their elastic behavior thus follows a membrane constitutive law with surface shear moduli G_{s_i}, surface dilatation modulus $3G_{s_i}$ and negligible bending resistance (Barthès-Biesel, 2016). The two capsules are filled with a Newtonian liquid (dynamic viscosity μ and density ρ). They are freely suspended in another Newtonian liquid (dynamic viscosity μ and density ρ), subjected to a steady simple shear flow with shear rate $\dot{\gamma}$. We use non-dimensional quantities throughout, with characteristic dimensions a for lengths, $1/\dot{\gamma}$ for time, $\mu\dot{\gamma}$ for viscous stress and G_{s_i} for elastic tensions (force per unit arc length) in the membrane of capsule C_i, respectively. We assume that the flow Reynolds number $\rho\dot{\gamma}a^2/\mu$ is very small, so that Stokes flow conditions prevail.

The undisturbed velocity field $\boldsymbol{v}^{\infty}$ is then

$$\boldsymbol{v}^{\infty} = y\,\boldsymbol{e_x}, \tag{1}$$

in the laboratory Cartesian reference frame (O, $\boldsymbol{e_x}$, $\boldsymbol{e_y}$, $\boldsymbol{e_z}$).

At time $t = 0$, the capsules are spherical and their centres of mass are positioned in the same shear plane, symmetrically with respect to the origin O of the laboratory reference frame (Fig 1). The objective of the numerical model is to follow the time evolution of the positions of the capsule centroids O_1 and O_2, with coordinates $\{x_i(t), y_i(t), z_i(t), i = 1, 2\}$, as well as the instantaneous deformation of each capsule. Note that for symmetry reasons in Stokes flow, the capsules remain in the initial shear plane, so that $z_i(t) = 0$: from now on, this parameter will be ignored. Typically, the capsules are first convected towards each other by the flow, eventually overpass and strongly interact and are finally convected away from each other. The computation is stopped when the two capsules are far enough to have regained the deformed shape they would take when alone in the shear flow.

The distance between the two centroids is defined by

$$\Delta x(t) = x_2(t) - x_1(t), \quad \Delta y(t) = y_2(t) - y_1(t) \tag{2}$$

The deformation and flow dynamics are governed by two non-dimensional parameters, such as the capillary numbers $Ca_i = \mu\dot{\gamma}a/G_{s_i}$, which compare the viscous to the elastic forces for each capsule. It is also convenient to introduce the ratio of shear moduli $\beta = G_{s_2}/G_{s_1} = Ca_1/Ca_2$. When $\beta < 1$, capsule C_1 is less deformable than capsule C_2 under identical flow conditions.

2.2. Fluid-structure interaction code

To solve the fluid-structure interaction problem, we do a Lagrangian tracking of the position of the capsule surfaces and couple iteratively the boundary integral method (BIM) solving for the fluid flows and the finite element method (FEM) solving for the membrane equilibrium (Walter et al., 2010). This method is similar to the one developed by C. Pozrikidis' group where BIM is coupled to the local solution of the membrane equilibrium equations on each membrane element (Pozrikidis, 1992; Ramanujan and Pozrikidis, 1998). To account for the interaction between the two capsules, we adapt the strategy developed by Hu et al. (2020) for two identical capsules.

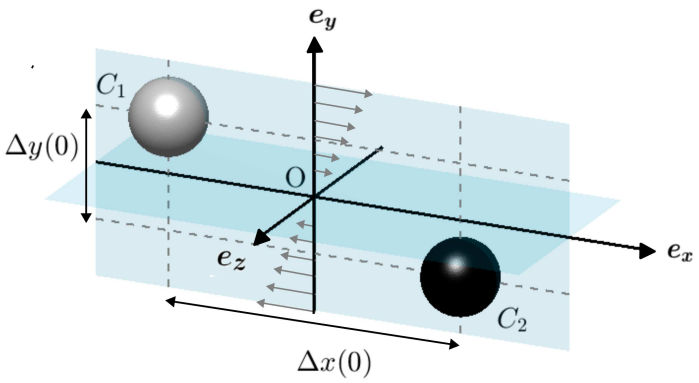

Figure 1: The two capsules are initially positioned in the same shear plane ($\boldsymbol{e_x}$, $\boldsymbol{e_y}$), with symmetrical positions with respect to the center of the laboratory reference frame.

2.2.1. Fluid flow

The motion of the capsules internal and external fluids is governed by the quasi-steady Stokes equations:

$$\nabla \cdot \boldsymbol{v}(\boldsymbol{x},t) = \boldsymbol{0}, \qquad \nabla \cdot \boldsymbol{\sigma}(\boldsymbol{x},t) = \boldsymbol{0}. \tag{3}$$

where $\boldsymbol{v}(\boldsymbol{x},t)$ is the velocity field and $\boldsymbol{\sigma}(\boldsymbol{x},t)$ is the fluid stress tensor given by Newton's law. Those equations can be put in an integral form that relates the velocity of the points of the capsule surfaces to the tractions on the membrane, at each time t:

$$\begin{aligned} \forall \boldsymbol{\xi} \in S_i(t), \qquad \boldsymbol{v}_i(\boldsymbol{\xi},t) = \boldsymbol{v}^{\infty}(\boldsymbol{\xi}) \quad &- \quad \frac{1}{8\pi Ca_1} \int_{S_1(t)} \boldsymbol{J}(\boldsymbol{\xi},\boldsymbol{\zeta}) \cdot \boldsymbol{q}_1(\boldsymbol{\zeta},t)\, dS(\boldsymbol{\zeta}) \\ &- \quad \frac{1}{8\pi Ca_2} \int_{S_2(t)} \boldsymbol{J}(\boldsymbol{\xi},\boldsymbol{\zeta}) \cdot \boldsymbol{q}_2(\boldsymbol{\zeta},t)\, dS(\boldsymbol{\zeta}), \end{aligned} \tag{4}$$

where $S_i(t)$ is the deformed surface of capsule C_i and $\boldsymbol{q}_i(\boldsymbol{\zeta},t)$ the membrane load on capsule C_i, at time t. The free space Green's function $\boldsymbol{J}$ is defined as:

$$\boldsymbol{J}(\boldsymbol{\xi},\boldsymbol{\zeta}) = \frac{\boldsymbol{I}}{\|\boldsymbol{\xi}-\boldsymbol{\zeta}\|} + \frac{(\boldsymbol{\xi}-\boldsymbol{\zeta}) \otimes (\boldsymbol{\xi}-\boldsymbol{\zeta})}{\|\boldsymbol{\xi}-\boldsymbol{\zeta}\|^3}, \tag{5}$$

with $\boldsymbol{I}$ the identity tensor.

Dynamic boundary conditions link the membrane load to the viscous stress jump $[\boldsymbol{\sigma}_i]$ across the membrane of capsule C_i

$$[\boldsymbol{\sigma}_i](\boldsymbol{\xi},t)\cdot\boldsymbol{n}=\frac{1}{Ca_i}\boldsymbol{q}_i(\boldsymbol{\xi},t),\qquad i=1,2\ (\text{no summation on}\,i) \tag{6}$$

where $\boldsymbol{n}$ the unit normal vector points outwards.

At a given time, the velocity fields are thus obtained directly using Eq. 4 knowing the values of the membrane load $\boldsymbol{q}_i$ provided at the previous instant by the solid solver (see the following subsection). Time t enters the problem through the kinematic conditions that relate the membrane velocities $\boldsymbol{v}_i$ to the time derivative of the displacement fields $\boldsymbol{u}_i$:

$$\forall\boldsymbol{\xi}\in S_i(t),\qquad \boldsymbol{v}_i(\boldsymbol{\xi},t)=\frac{\partial}{\partial t}\boldsymbol{u}_i(\boldsymbol{\xi},t),\qquad i=1,2. \tag{7}$$

Finally, Eq. 7 is integrated in time using a second-order Runge-Kutta Ralston scheme to update the displacement fields $\boldsymbol{u}_i$.

2.2.2. Capsule wall mechanics

For both capsules, the thickness of the membrane is assumed to be negligible with respect to the radius a. As mentioned above, we further assume that the membrane mechanical properties are governed by a neo-Hookean constitutive law, appropriate for an infinitely thin sheet of a three-dimensional isotropic volume incompressible material devoid of bending resistance (see Barthès-Biesel (2016) for details). The strain energy w_i per unit undeformed surface area is then given by:

$$w_i=\frac{1}{2}\left[\lambda_{\mathrm{I}}^2+{\lambda_{\mathrm{II}}}^2-3+\frac{1}{{\lambda_{\mathrm{I}}}^2{\lambda_{\mathrm{II}}}^2}\right], \tag{8}$$

where λ_{I} and λ_{II} are the two principal extension ratios of the membranes of each capsule (for clarity, the subscript corresponding to the capsule has been omitted in the notations for the extension ratios). Note that w_i is scaled with aG_{s_i} and thus corresponds to an intrinsic property of capsule C_i.

At each time t, the membrane equilibrium on the deformed surface of each capsule reads:

$$\boldsymbol{q}_i+\nabla_s\cdot\boldsymbol{T}_i=0,\qquad i=1,2, \tag{9}$$

where ∇_s denotes the surface gradient operator and $\boldsymbol{T}_i$ the Cauchy tension tensor in the membrane.

Equations 9 can be rewritten using the virtual work principle:

$$\int_{S_i(t)} \hat{\boldsymbol{u}}_i \cdot \boldsymbol{q}_i \, dS = \int_{S_i(t)} \hat{\boldsymbol{e}}_i : \boldsymbol{T}_i \, dS, \qquad i = 1, 2, \tag{10}$$

where $\hat{\boldsymbol{u}}_i$ is an arbitrary kinematically admissible virtual displacement and $\hat{\boldsymbol{e}}_i$ the corresponding virtual strain tensor. This principle dictates that the virtual work done by the external loads acting on a deformable body is equal to the virtual change in internal strain energy. Using the values of $\boldsymbol{u}_i$ provided by the fluid solver, we can compute the deformation, the strain energy w_i and the Cauchy tensions $\boldsymbol{T}_i$ for each capsule membrane. Eq. 10 is then discretized and solved for $\boldsymbol{q}_i$, which is given to the fluid solver for a new iteration (Walter et al., 2010; Barthès-Biesel et al., 2010).

2.2.3. Deformation energy and capsule damage

The novel aspect of the present study is that we take into account the possibility of membrane damage for the capsules. In the framework of the theory of continuum damage mechanics (CDM), one mechanical property of the capsule membrane material is Y_D, the threshold deformation energy density in the membrane, above which damage occurs (Kachanov, 1986; Lemaitre and Desmorat, 2005). Correspondingly, damage is induced as soon as

$$w_i^m(t) \geq Y_D, \qquad i = 1, 2, \tag{11}$$

where $w_i^m(t)$ is the maximum of the deformation energy density on the membrane at time t.

Recently Grandmaison et al. (2021) have used the CDM theory to develop a macro-scale model of the onset and time evolution of damage in the membrane of a single capsule flowing in a simple shear flow. They provide the relation between Y_D and the critical capillary number Ca_c above which damage occurs. Their maximum damage criterion is $Y_D = 0.7$, which corresponds to $Ca_c = 1$. Note that it is difficult to reach a stable state for $Ca \geq 1$ for a capsule with a neo-Hookean membrane (Lac et al., 2004; Walter et al., 2010; Wang et al., 2021). We have used this same damage criterion $Y_D = 0.7$ throughout the interaction. The effect of the choice of a lower value of Y_D is discussed in section 4. Furthermore, since the objective of the present work is to determine whether capsule damage is induced during crossing but not to predict its evolution, we have not implemented the full damage evolution model.

In order to assess the relative effect of the hydrodynamic interaction on the capsule deformation, we use as a reference, the situation where the capsules are far enough from each other and behave as if they were alone in a simple shear flow with

relative strength Ca_i. The reference deformed profiles and the value of the maximum energy density w^m_{ref} are determined as a function of Ca by solving Eq. 4 for only one capsule (i.e. by integrating over $S_1(t)$ and setting to zero the integral over $S_2(t)$) and taking the value at steady state (Fig. 2).

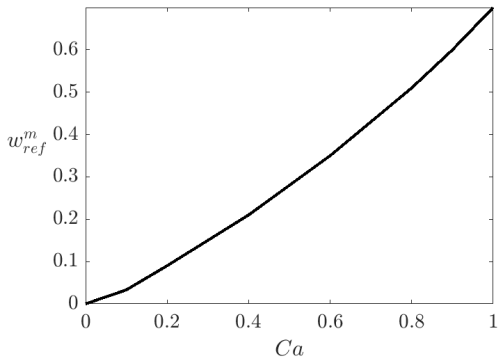

Figure 2: Maximum deformation energy density w^m_{ref} for a single capsule in simple shear flow at steady state.

2.2.4. Numerical set-up and validation

We discretize the capsules membranes with a triangular mesh and follow the surface nodes position over time. At a given time t, two integral equations corresponding to Eq. 4 are solved to yield the velocity of the capsule nodes. The velocities are then integrated (Eq. 7) to yield the displacement field of the nodes at time $t + \Delta t$, where Δt is the time step. The new position of the membrane points is transmitted to the solid solver. The solution of Eq. 10 yields the value of the load $\boldsymbol{q}_i$ at the nodes of the capsule surfaces. The process is then repeated until a typical total interaction time $t_f = 45$. The numerical code gives the capsule deformed profiles at each time. Post treatment of the data allows us to compute the trajectories of the capsule centroids O_i as well as the time evolution of the elastic energy and stresses in the capsule membranes.

Since the numerical method is explicit, it is very important to verify the precision of the capsule centroid trajectories. The numerical code is identical to the one used by Hu et al. (2020) to study the motion of two identical capsules initially located in two different shear planes. The only difference is that Hu et al. (2020) had to solve only one integral equation (Eq. 4), in which the two integrals could be collapsed into one, since the capsules were identical. In our case, the computation is a little more complex as we have to solve two integral equations (Eq. 4 for each capsule)

containing two integrals. The procedure is thus more time consuming. Hu et al. (2020) have studied the influence of the time step and of the mesh size on the capsule surface. They concluded that with a surface mesh of 1280 P2 elements and 2562 nodes (with characteristic mesh size $O(0.1a)$) and a time step $\Delta t = 5 \times 10^{-4}$, the error on the trajectories of the capsule centroids was of order 0.05 at the end of the interaction, i.e. at a final time of order $t \geq 100$. For $\beta = 1$ and $Ca_2 = 0.3$, the capsule centroid trajectories obtained with our code and those obtained by the code of Hu et al. (2020), differ by less than 0.02. Correspondingly, in all that follows, we have thus used 1280 P2 elements on each capsule and a time step of 5×10^{-4}. This also ensures a precision of order 10^{-2} for the Taylor deformation of the profiles and for the deformation energy density w (Walter et al., 2010; Dupont et al., 2015).

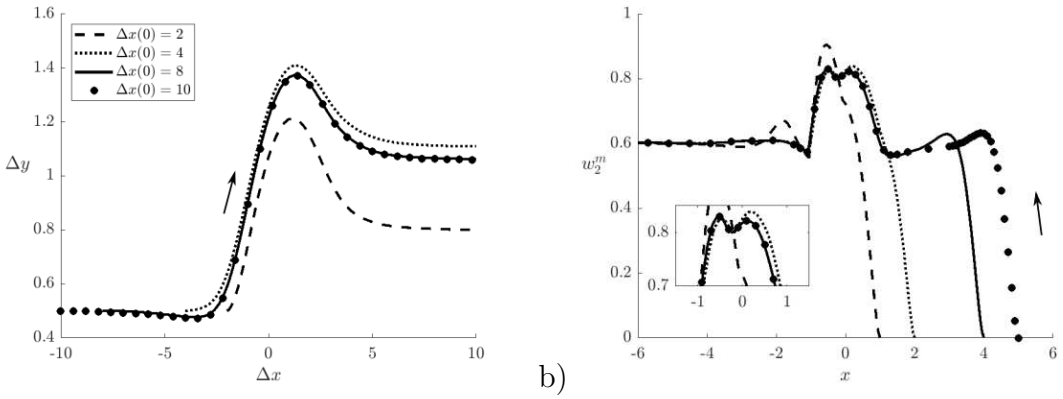

Figure 3: Influence of the initial position $\Delta x(0)$ on the interaction of two different capsules for $\beta = 1/3, Ca_2 = 0.9$. (a) Relative trajectory of the capsules centroids; (b) Maximum deformation energy density of C_2 as a function of O_2 position. A zoom on the maximum has been inserted at the bottom left of the figure. The arrows indicate the direction of time evolution.

It is also important to ensure that the results are independent of the initial condition $\Delta x(0)$. To illustrate this point, we consider the case $\Delta y(0) = 0.5$, $\beta = 1/3$, $Ca_2 = 0.9$ and vary $\Delta x(0)$ between 2 and 10. Fig. 3a shows that the relative trajectory of the two capsules centroids are independent of initial conditions for $\Delta x(0) \geq 8$. The same conclusion is reached if we consider the evolution of the maximum deformation energy density w_2^m stored in the membrane of C_2 (Fig. 3b): the peak of energy, and thus of deformation, depends significantly on the initial conditions for $\Delta x(0) < 4$. Note that the same conclusion also applies to the effect of $\Delta x(0)$ on the variation of w_1^m along the trajectory of C_1. But as w_1^m is smaller than w_2^m, the effect is small and thus not shown.

Consequently, in all the present results, great care has been taken to ensure

$\Delta y(0)$	$\Delta x(0)$
0.2	10
1	24
2	28

Table 1: Influence of $\Delta y(0)$ on the values of $\Delta x(0)$ necessary to reach a steady state before capsules interaction.

that each capsule has reached the reference steady deformation, before it enters the interaction zone. Specifically, this means that we impose

$$|w_i^m(t) - w_{ref}^m(Ca_i)|/w_{ref}^m(Ca_i) \leq 0.02 \quad \text{for} \quad \Delta x = 0.2, \qquad i = 1, 2 \qquad (12)$$

With this criterion, we have evaluated the interaction zone to extend over $\Delta x \sim 4$. The value of $\Delta x(0)$ depends on $\Delta y(0)$: the greater $\Delta y(0)$, the greater $\Delta x(0)$ as shown in Table 1. This dependency is rather complex and nonlinear. Indeed, as $\Delta y(0)$ increases, the relative velocity of the two capsules increases and the time to reach the reference state w_{ref}^m necessitates a longer distance along $\boldsymbol{e}_x$: thus $\Delta x(0)$ increases too. On the other hand, as $\Delta y(0)$ increases, the strength of the interaction between the capsules decreases and the length of the interaction zone along $\boldsymbol{e}_x$ decreases.

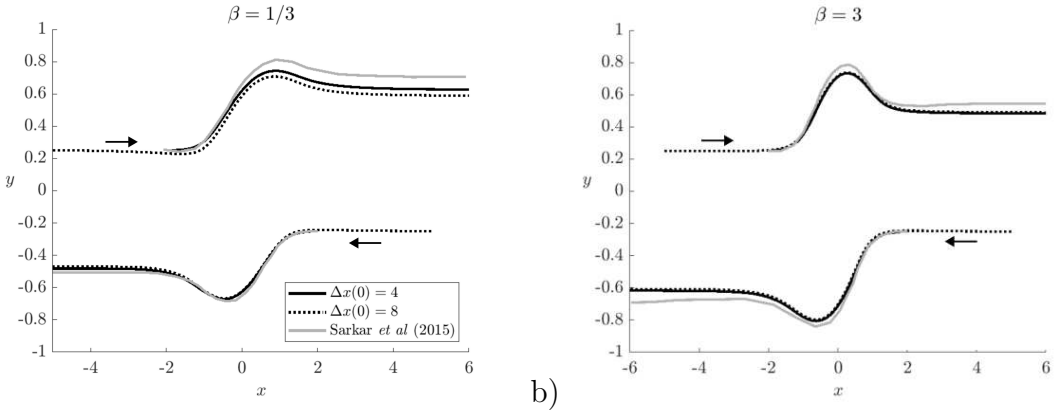

a) b)

Figure 4: Trajectories of the centroids of two interacting capsules for $Ca_1 = 0.3$, $\Delta y(0) = 0.5$ and $\Delta x(0) = 4$: results of Singh and Sarkar (2015) (grey line), present study (full dark line) for (a) $\beta = 1/3$ and (b) 3. We provide additional trajectories for $\Delta x(0) = 8$ (dotted line). The black arrows indicate the directions of time evolution.

We have compared our results to those obtained by Singh and Sarkar (2015) for $Ca_1 = 0.3$, $\Delta x(0) = 4$, $\Delta y(0) = 0.5$, in the cases of $\beta = 1/3$ (Fig. 4a) and $\beta = 3$ (Fig. 4b). We find that the maximum difference on the capsules trajectories is about

0.08 when $\beta = 1/3$ and a little less for $\beta = 3$. However, the centroid distances along the flow direction, chosen by Singh and Sarkar (2015) are too small to obtain results that are independent of the initial position for $\beta = 1/3$. But, if we use $\Delta x(0) = 8$, the capsule trajectories become independent of the initial conditions. However, the maximum difference on the trajectories between our results and those of Singh and Sarkar (2015) increases to 0.1. When $\beta = 3$, $\Delta x(0) = 4$ is sufficient for the capsules to reach a steady state before interacting, but a maximum difference on the capsules trajectories of 0.05 is still observed.

3. Dynamics of capsule crossing

3.1. Analysis of a typical capsule interaction

We consider the case $Ca_2 = 0.1$ and $\beta = 4$ as a typical case. Capsule C_1 is then 4 times softer than C_2 and is subjected to a baseflow capillary number $Ca_1 = 0.4$ (see Movie 1). The centroids initial separation is $\Delta x(0) = 10$, $\Delta y(0) = 0.2$. The capsules are thus convected towards each other. The centroids trajectories in the shear plane are shown in Fig. 5a. On selected points along the trajectories (corresponding to given instants t), the deformed profiles of the two capsules are compared to the reference profiles of the single capsule flowing at the corresponding value of Ca_i. When the flow is started and after an initial transient, both capsules deform and take a tank-treading motion as if they were alone. Consequently, before interaction, a perfect superposition of the deformed profiles (profiles (i)) with the respective reference profiles is observed for $x_1 = -4$ and $x_2 = 4$: the presence of the other capsule has no influence on the dynamics. Furthermore, we can note that the two capsules have reached a deformed state that is independent of their initial position.

As the capsules become closer, they enter the hydrodynamic interaction zone and their trajectories deviate from straight lines. As shown in Fig. 5a, this occurs roughly for $x_1 > -2$ and $x_2 < 2$. The centroids are then displaced along the velocity gradient direction, so that the two capsules can overpass (recall that their centroids remain in the shear plane). At the peak of interaction (profiles (j) and (k)), there is a thin lubrication film between the two capsules (Fig. 5b). The high pressure exerted in the lubrication film significantly deforms the capsule profiles, which are no longer ellipsoidal. A curvature inversion may even occur (profiles (j) and (k)). The presence of this lubrication film prevents contact between the capsules, so that it is not necessary to introduce a phenomenological repulsion force between the particles. This phenomenon has also been reported by Lac et al. (2007). Capsule C_1 is more deformed than capsule C_2 because of its lower rigidity. As the capsules are convected away from each other, they regain their respective reference deformed shapes (profiles

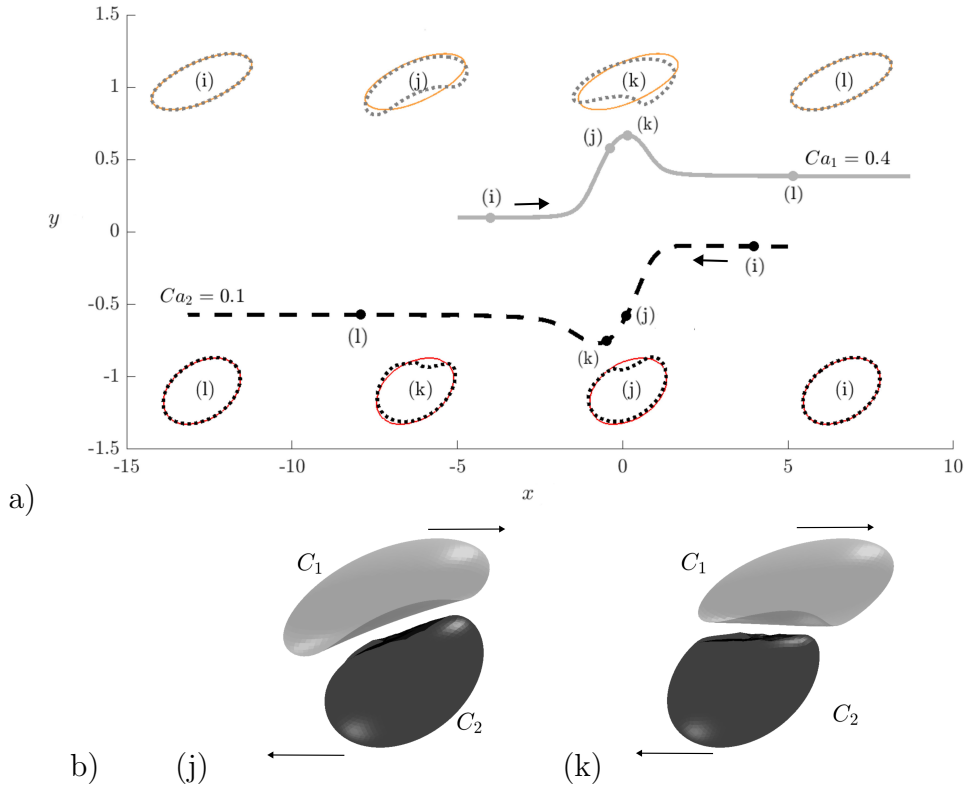

Figure 5: (a) Trajectories of the capsule centroids within the shear plane for $Ca_2 = 0.1$, $\beta = 4$, $\Delta y(0) = 0.2$, $\Delta x(0) = 10$ and a total interaction time $t_f = 60$. The black arrows indicate the direction of time evolution. Capsule profiles in the shear plane are shown (i) before interaction ($t = 6.6$), (j) at w_1^M ($t = 36.6$), (k) at the maximum separation Δy ($t = 37.6$), and (l) after interaction ($t = 58.8$). The reference profile of a single capsule flowing at the corresponding Ca is represented with an orange solid line for C_1 and a red solid line for C_2 in each insert. (b) Three-dimensional deformed capsules at instant (j) and (k), corresponding to the maximum deformation of C_1 and C_2, respectively.

(l)), but their centers are on streamlines that are different from the initial ones: this is due to the fact the Stokes flows are not reversible when deformable objects are freely suspended. This irreversible trajectory shift depends on the capsule rigidity and decreases as Ca increases. As a consequence C_2 moves faster than C_1: this is why the trajectories on Fig. 5a do not have the same length whereas they are ended at the same time $t_f = 60$. This phenomenon creates self diffusion effects in a capsule suspension.

The variation of the maximum deformation energy density of each capsule during

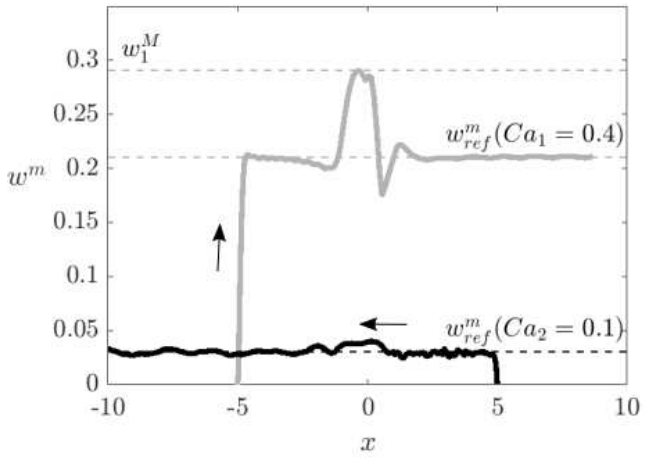

Figure 6: Evolution of the maximum energy density w_i^m as a function of the centroid position x_i for both capsules ($\beta = 4$, $Ca_2 = 0.1$, $\Delta y(0) = 0.2$). Dash lines: reference values $w^m_{ref}(Ca_i)$. The arrows indicate the direction of time evolution. The maximum value over time w_1^M is reached at $t = 36.6$ corresponding to $x_1 = -0.38$ and $x_2 = 0.11$.

the interaction is shown in Fig. 6. Since capsule C_2 is more rigid (and less deformed) than C_1, $w_1^m(t) > w_2^m(t)$. The values of $w_i^m(t)$ are equal to $w^m_{ref}(Ca_i)$ before and after the close interaction. During interaction, the membrane maximum energy densities $w_i^m(t)$ reach a maximum value w_i^M and then decrease in a damped manner towards the reference value. The close encounter of the two capsules thus creates transient excess tensions in the capsule membrane, which may lead to damage. This phenomenon will be studied in detail in section 4.

3.2. Influence of the difference in capsule rigidity β and flow conditions

Keeping the flow conditions for C_2 constant ($Ca_2 = 0.1$, $\Delta y(0) = 0.2$, $\Delta x(0) = 10$), we now vary the values of the rigidity ratio β. The corresponding deformed profiles are shown at the maximum of w_2^m in Fig.7a, for $\beta = 1, 3, 9$. Note that the centers are not simultaneously at $x = 0$ when $\beta \neq 1$: this is due to the difference of trajectory shift of each capsule, as previously discussed. For $\beta = 1$, the two capsules have identical deformed shapes, as expected. As β increases, the deformability of C_1 increases too. During the close interaction, C_1 has to flow around the comparatively rigid capsule C_2 and is stretched in the process. This is particularly evident for $\beta = 9$, where C_1 is much elongated whereas C_2 barely changes shape.

Now, keeping the same deformability ratio ($\beta = 3$) and flow conditions ($Ca_2 = 0.1$), we vary the initial capsule separation and consider $\Delta y(0) = 0.2, 1$ and 2 (Fig.

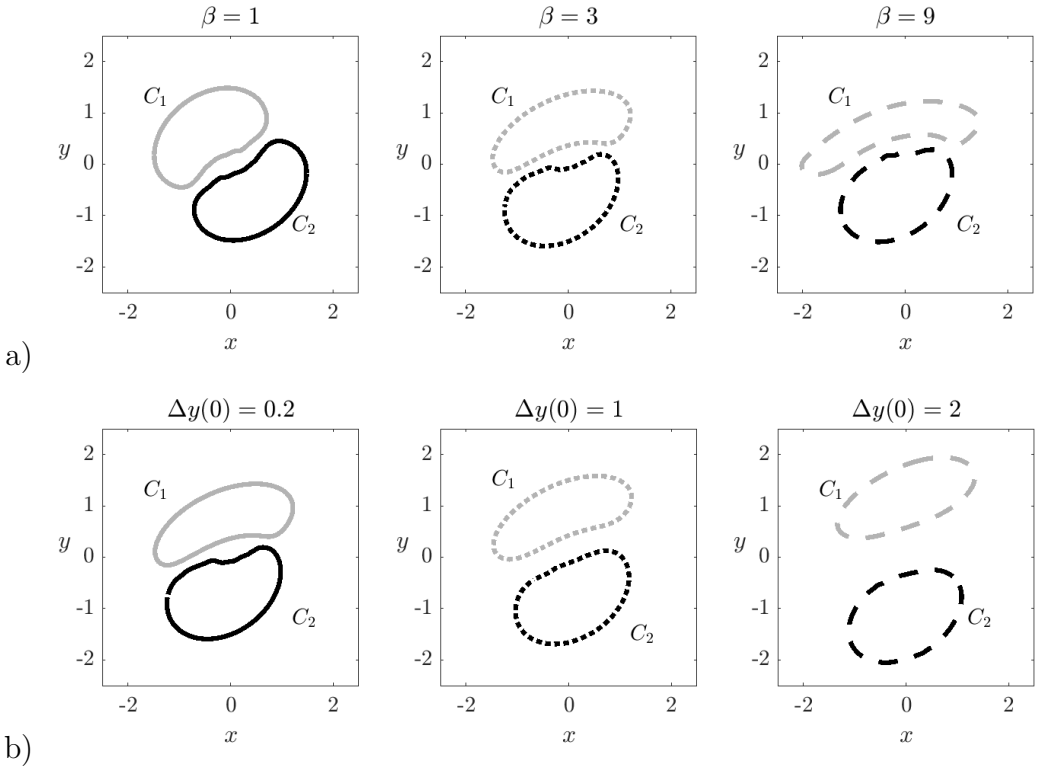

Figure 7: Capsule profiles in the shear plane for $Ca_2 = 0.1$ for w_1^M. (a) Influence of β for $\Delta y(0) = 0.2$; (b) Influence of $\Delta y(0)$ for $\beta = 3$.

7b). When the two capsules are nearly on the same initial streamline ($\Delta y(0) = 0.2$), the deformation of both capsules differs significantly from the reference (as is evidenced by the increase in w_i^m, shown in Fig 6). This is due to the fact that the lubrication film between the capsules is thin and large pressure forces thus develop and deform the capsules. However, as we increase the initial streamline separation, the lubrication film becomes wider during crossover, the pressure forces decrease and the two capsules have deformed profiles that become very near the reference ones as shown in Fig. 7b for $\Delta y(0) = 2$.

We can also analyze the self diffusion effect in the suspension. In Fig. 8, we show the irreversible increase of capsule separation $\Delta y(\infty) - \Delta y(0)$ due to the interaction. We note that the deviation is largest when the two capsules are on close streamlines (almost frontal collision), corresponding to $\Delta y(0) = 0.2$. In that case, there is a clear effect of capsule rigidity: the deviation is larger for rigid particles that for soft ones. This phenomenon is evidenced by the decrease of the deviation with β and by the

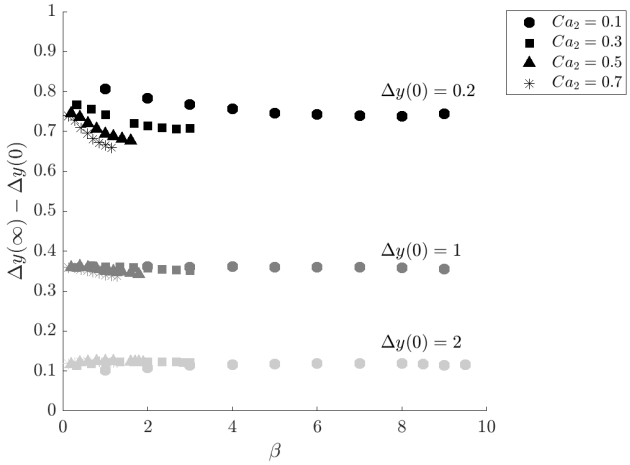

Figure 8: Influence of $\Delta y(0)$, β and Ca_2 on the capsule self-diffusion in the shear plane.

ordering of the curves with Ca_1. However, for large initial separation ($\Delta y(0) \geq 0.5$), there is no effect of the flow conditions nor of deformability mismatch. This later point was noted by Singh and Sarkar (2015), who proposed a correlation where the final deviation of C_1, normalized by the final deviation for two identical capsules depended linearly on $\beta^{-0.6}$. We have been unable to reproduce this correlation. This may be due to the difference in the capsule trajectories, as discussed in section 2.2.4.

In all the above cases, the time evolution of the maximum deformation energy density $w_i^m(t)$ is similar to the one shown in Fig. 6. It is then best characterized by the peak value for each capsule w_i^M. Correspondingly, we show the coupled influence of flow conditions (measured by Ca_2) and deformability difference β on w_i^M in Fig. 9. We did not consider large values $Ca_i > 1$ which might lead to membrane instability (see section 2.2.3) or low values $Ca_i < 0.1$, which correspond to nearly rigid capsules. In all cases, the interaction leads to values of w_i^M that are above the reference level that would prevail if the capsule were alone. Note that we checked that considering $\Delta y(0) = 0$ instead of 0.2 yielded essentially the same results for w_i^m, but for a significantly larger computational cost. Furthermore, for an initial cross streamlines separation of one diameter or more ($\Delta y(0) \geq 2$), there is very little interaction effect, i.e. the capsules do not experience much extra deformation when they cross. The results in Fig. 9a can also be represented by a mapping of the maximum values of w^M (whether the maximum is reached for C_1 or C_2) in the Ca_1, Ca_2 space, as shown in Fig. 10.

The charts in Fig. 9 and 10 are an important novel result of this study, as they

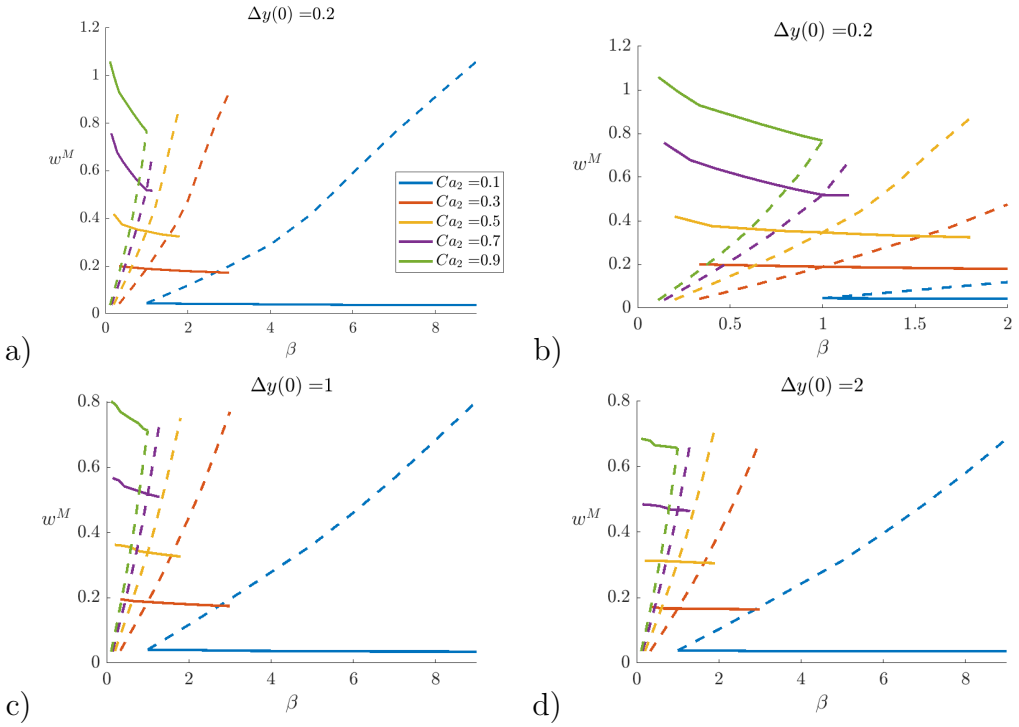

Figure 9: Charts of the maximum deformation energy density w_i^M for a given constant value of Ca_2 and varying values of β. Solid line: w_2^M; Dotted line: w_1^M. (a) Low initial separation $\Delta y(0) = 0.2$; (b) Zoom on low values of β for $\Delta y(0) = 0.2$; (c) Medium initial separation $\Delta y(0) = 1$; (d) Large initial separation $\Delta y(0) = 2$.

allow us to quantify exactly the effect of the interaction on the deformation energy level.

4. Capsule membrane damage due to interaction

We now study in detail the role of differences in membrane properties on the possibility of damage occurrence. As an example (see Movie 2), we consider a fairly rigid capsule ($Ca_2 = 0.1$) and a very deformable one ($Ca_1 = 0.8$). If they were alone in the flow, both capsules would be subjected to flow conditions that are below the damage limit $Ca_c = 1$. However, when they interact, the situation changes completely, as shown in Fig. 11, where the maximum deformation energy density of each capsule is represented as a function of position. The motion and deformation of C_2 is barely affected by the presence of C_1. On the other hand, C_1 first reaches a steady deformed profile for $x_1 > -4$, with a maximum deformation energy density

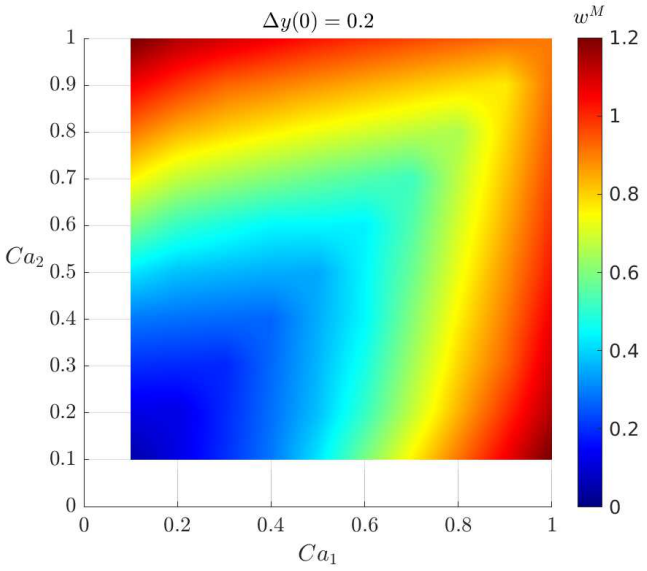

Figure 10: Maximum value of w^M (whether the maximum is reached for C_1 or C_2) for $\Delta y(0) = 0.2$.

$w_1^m = w_{ref}^m(Ca_1 = 0.8) = 0.51$, which is less than the damage limit $Y_D = 0.7$. However, during close interaction, C_1 is highly deformed (Fig. 11) and its deformation energy reaches a maximum value of order $w_1^M = 0.92$, which is much larger than Y_D. We may expect in this case that capsule C_1 will be damaged by the interaction.

In order to analyze where the damage occurs, we perform a Lagrangian tracking of the material points of C_1 membrane for which $w_i \geq Y_D$ at a given time. We use different grey levels at different instants to show how the damaged region evolves in shape over time, as shown in Fig. 12. Damage first initiates around the intersection of the membrane with the vorticity axis as in the case of a single capsule in shear flow (Grandmaison et al., 2021). However, during interaction the damage zone extends over most of the top (i.e. opposite to C_1) equatorial area of C_2. Note that the motion modulates the shape of the zone damaged at a previous instant of time. Altogether, some membrane elements are subjected to deformation energy levels higher than Y_D, for a duration up to 2.6. As shown by Grandmaison et al. (2021) for a single capsule subjected to a constant shear flow, once damage is initiated, the density of defects in the membrane increases with time, until either a steady damaged state or rupture is reached. This occurs over durations of order 2.5, which are comparable to the time

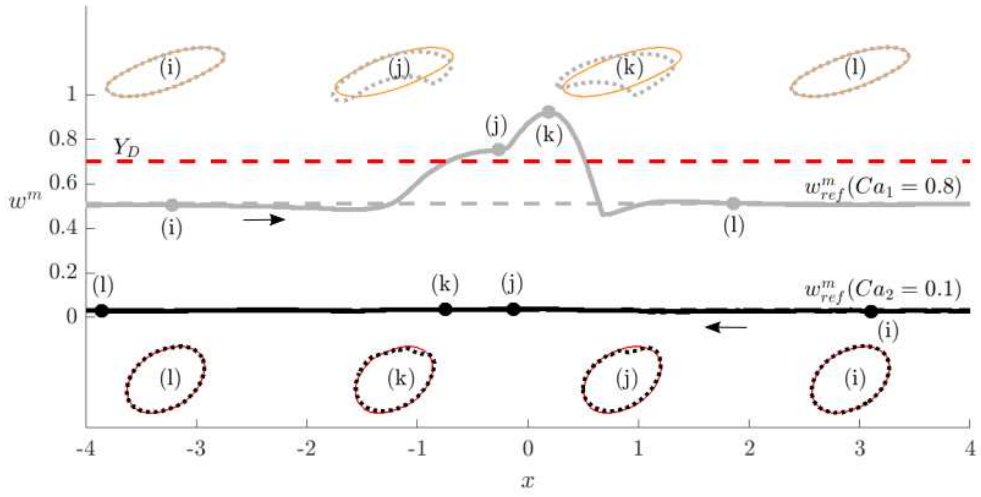

Figure 11: Damage of two interacting capsules with membrane different properties $\beta = 8$ for $Ca_2 = 0.1$, $\Delta x(0) = 10, \Delta y(0) = 0.2$: maximum deformation energy density w_i^m as a function of x_i. Capsule profiles in the shear plane are shown before interaction (i), just after damage initialization (j), at w_1^M (k) and after interaction (l). The reference profile of a single capsule flowing at the corresponding Ca is represented in orange solid line for C_1 and red solid line for C_2 in each insert.

of exposition to damaging tensions determined above for C_2. We may then expect that defects will develop on the membrane of C_2.

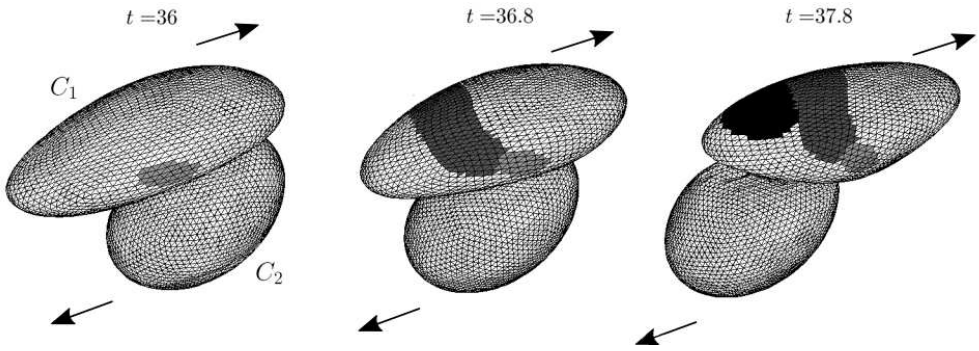

Figure 12: Lagrangian tracking of the damage zone ($w_i^M > Y_D$) of two interacting capsules with different membrane mechanical properties ($\beta = 8$, $Ca_1 = 0.8$, $\Delta x(0) = 10, \Delta y(0) = 0.2$). A different grey level is used for each time step. The times $t = 36.8$ and $t = 37.8$ correspond to instants (j) and (k) in Fig. 11, respectively. The arrows indicate the direction of shear.

Those results are important because they indicate that unexpected damage may

occur in a suspension due to interactions only. In order to quantify this phenomenon, we compare the values of w_i^M defined in Fig. 9 or 10 to the damage threshold Y_D, and build phase diagrams that show when damage should be expected as a function of the respective capillary numbers of the two capsules. Specifically, using the damage threshold $Y_D = 0.7$, $Ca_c = 1$ and close interactions ($\Delta y(0) = 0.2$), we obtain the phase diagram shown in Fig. 13. When $Ca_i \geq 1$, the baseflow itself may lead to damage (dark zone). When both Ca_1 and Ca_2 are small enough, no damage will occur even when the capsules interact (white zone). However, there is a grey zone where damage is occurring due to interactions only. The interaction damage is more likely to occur when the capsules have very different properties. Note that for the sake of simplicity, we have delimited the border between the grey and white zones with a straight line. We could have used a more sophisticated criterion based for example on the difference $|w_i^M - Y_D|$, but the general picture would not have been changed significantly. Furthermore, the corresponding slight displacement of the border would have been within the numerical precision.

We assess the effect of the initial separation between the capsules on interaction damage zone by increasing $\Delta y(0)$ to 2 (Fig. 14a). When the initial separation increases, the interaction damage zone becomes smaller because interactions are weaker. We can also consider the effect of the damage limit for $\Delta y(0) = 0.2$. For more fragile capsules corresponding, for example, to $Y_D = 0.4$, the boundaries of the phase diagram are correspondingly modified as shown in Fig. 14b. In that case, the no damage zone domain is considerably diminished.

5. Discussion and conclusion

Using a fluid-structure interaction code coupling the finite element and boundary integral methods, we have modeled the interaction between two capsules placed in a simple shear flow. We have investigated how their trajectory and membrane tensions are impacted by the mechanical properties of the capsule wall, especially when the latter differ from one capsule to the other. This case is of particular interest, as it is typical in capsule suspensions. Particle close interactions lead to peaks in membrane tension, that may exceed the capsule damage limit and lead to rupture.

Some pre-existing studies on capsule interactions in shear flow have used a numerical approach based on finite differences and immersed boundaries which allows one to consider non-Newtonian fluids and inertial flow conditions (Singh and Sarkar, 2015; Doddi and Bagchi, 2008). The drawback is that the computational domain must be large enough to verify the far field boundary conditions with accuracy. Indeed, Singh and Sarkar (2015) have checked that the width of the fluid domain along

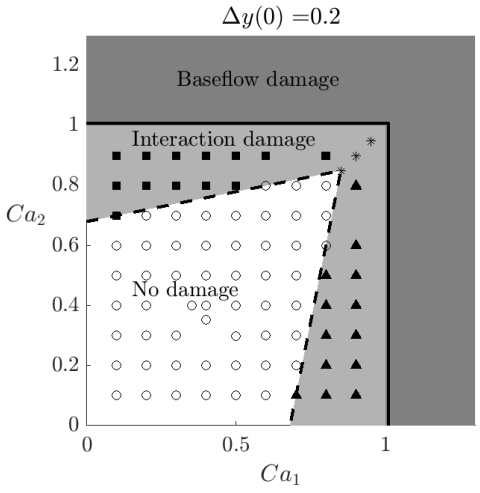

Figure 13: Phase diagram of capsule damage as a function of Ca_1 and Ca_2 for $\Delta y(0) = 0.2$, $Y_D = 0.7$ ($Ca_c = 1$). All the symbols represent a numerical run: ▲ C_1 damaged, ■ C_2 damaged, $*$ C_1 and C_2 damaged.

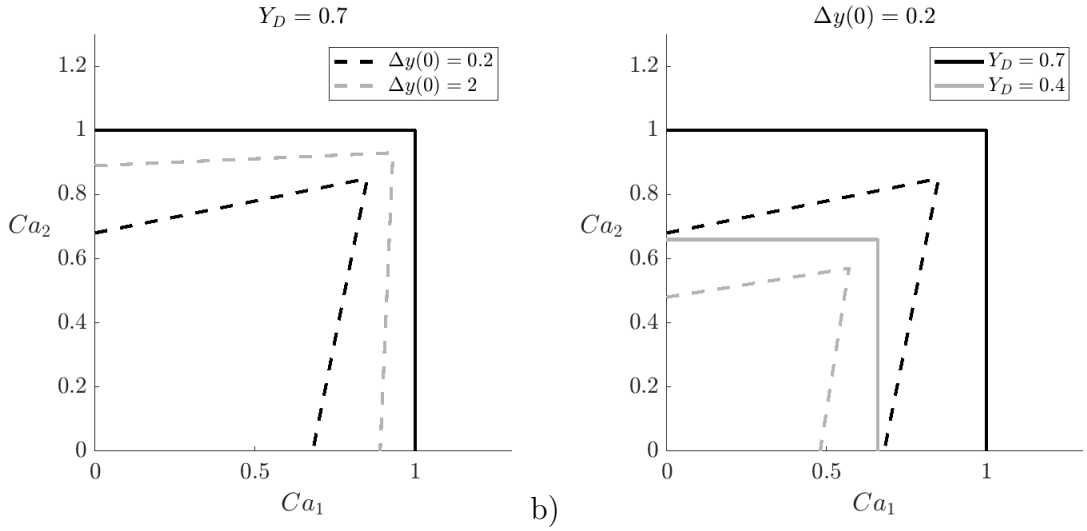

Figure 14: Influence of (a) the initial separation $\Delta y(0)$ ($Y_D = 0.7$) and (b) the energy criterion Y_D ($\Delta y(0) = 0.2$) on the damage limits. Solid lines: lower limit of base flow damage; Dash lines: lower limit of interaction damage. The two solid lines are superimposed on (a).

the velocity gradient direction was large enough to have no influence on the trajectories of the interacting capsules. However, the length of the domain in the flow direction also has to be long enough to avoid the interaction results to be initial

state dependent. This point is rarely checked. The advantage of our fluid–structure interaction numerical code is that the flow domain is infinite with exact boundary conditions of vanishing perturbation on the outer boundary. The drawback is that it is limited to Newtonian fluids undergoing flows with negligible inertia.

We used the spherical rest shape as the initial condition, thus following the usual procedure. However, if we want crossing results that do not depend on the initial positions of the capsules, we have to position them far enough so that they reach their equilibrium shape before starting to interact. This procedure is absolutely necessary to get results that do not depend on the initial state of the system. This point is very important, but has rarely been taken into account in previous studies.

Our interaction results account for almost head on collisions and cover a wide range of capillary numbers and capsule properties mismatch. We have chosen to analyze the capsule deformation in terms of elastic energy rather than a Taylor deformation parameter, that is a pertinent measure for nearly ellipsoidal shapes but not for highly asymmetric profiles such as those shown in Fig. 5, 7 and 11. As was previously noted by Singh and Sarkar (2015), the difference in capsule membrane rigidity only has a small influence on the trajectory shift after collision (Fig. 8): the main effect is the collision type. Not surprisingly, we find that the shift is larger for a head on collision than for a grazing one.

The main result of this paper is the new data that we give on the transient deformation energy in the membrane of the two capsules at the peak of interaction. The findings are gathered in the charts of Fig. 9. Those charts can be used to build phase diagrams similar to Fig. 14b for any appropriate value of damage threshold in deformation energy density Y_D. They show that particle close interactions can be responsible for damage initiation on the capsule membrane and that damage has enough time to evolve during the capsule motion. The time during which the energy density exceeds Y_D is indeed of the same order of magnitude than in Grandmaison et al. (2021).

The phase diagrams can be used by experimentalists to determine the safe flow conditions for a suspension of capsules with a dispersion of mechanical properties. They can also be used to sort out capsules that are too soft. For example, if one subjects a suspension of cells C_2 to harmless flow conditions (e.g. $Ca_2 = 0.2$), the phase diagram in Fig. 13 shows that all the cells with an elastic modulus G_{s1} less than $G_{s2}/3.5$ might be damaged because of hydrodynamic interactions. This value of G_{s1} is significantly higher than the one ($G_{s2}/5$) that would be obtained by considering base flow induced damage only. Conversely, if cells C_2 are subjected to a high shear (e.g. $Ca_2 = 0.8$), they will be damaged by a collision with hard particles (with the same size) in the suspension. The two phenomena may explain why cell damage

is observed in needle delivery systems where high shear rates prevail near the walls (Aguado et al., 2012; Wahlberg et al., 2018; Chen et al., 2022).

Note that we have built the phase diagrams assuming the same value of Y_D for the two capsules. But, Y_D could well vary with G_s and not have the same value for the two capsules. However, we are not aware of any data on this issue. Note also that the two capsules have been assumed to have the same size. The interaction of two capsules with different diameters is in progress.

6. Acknowledgements

This project received funding from Région Hauts-de-France (STaRS project which supports young scientific experts) and from the European Research Council (ERC) under the European Union's Horizon 2020 research and innovation programme (Grant agreement No. ERC-2017-COG - MultiphysMicroCaps).

References

Aguado, B. A., Mulyasasmita, W., Su, J., Lampe, K., Heilshorn, S. C., 2012. Improving viability of stem cells during syringe needle flow through the design of hydrogel cell carriers. Tissue Eng. Part A 18 (7-8), 806–815.

Barthès-Biesel, D., 1991. Role of interfacial properties on the motion and deformation of capsules in shear flow. Physica A 172, 103 – 124.

Barthès-Biesel, D., 2016. Motion and deformation of elastic capsules and vesicles in flow. Annu. Rev. Fluid Mech. 48 (1), 25–52.

Barthès-Biesel, D., Walter, J., Salsac, A.-V., 2010. Computational hydrodynamics of capsules and biological cells. Taylor & Francis, Ch. Flow-induced deformation of artificial capsules, pp. 35–70.

Carin, M., Barthès-Biesel, D., Edwards-Lévy, F., Postel, C., Andrei, D. C., 2003. Compression of biocompatible liquid-filled HSA–alginate capsules: Determination of the membrane mechanical properties. Biotechnol. Bioeng. 82, 207 – 212.

Chang, K. S., Olbricht, W. L., 1993a. Experimental studies of the deformation and breakup of a synthetic capsule in extensional flow. J. Fluid Mech. 250, 587 – 608.

Chang, K. S., Olbricht, W. L., 1993b. Experimental studies of the deformation and breakup of a synthetic capsule in steady and unsteady simple shear flow. J. Fluid Mech. 250, 609 – 633.

Chen, B. Z., Zhao, Z. Q., Shahbazi, M.-A., Guo, X. D., 2022. Microneedle-based technology for cell therapy: current status and future directions. Nanoscale Horiz. 7 (7), 715–728.

de Loubens, C., Deschamps, J., Georgelin, M., Charrier, A., Edward-Lévy, F., Leonetti, M., 2014. Mechanical characterization of cross–linked serum albumin microcapsules. Soft Matter 10, 4561 – 4568.

Doddi, S. K., Bagchi, P., 2008. Effect of inertia on the hydrodynamic interaction between two liquid capsules in simple shear flow. Int. J. Multiphase Flow 34, 375 – 392.

Dupont, C., Salsac, A.-V., Barthès-Biesel, D., Vidrascu, M., Tallec, P. L., 2015. Influence of bending resistance on the dynamics of a spherical capsule in shear flow. Phys. Fluids 27 (5), 051902.

Ghaemi, A., Philipp, A., Bauer, A., Last, K., Fery, A., Gekle, S., 2016. Mechanical behaviour of micro-capsules and their rupture under compression. Chem. Eng. Sci. 142, 236–243.

Gires, P.-Y., Srivastav, A., Misbah, C., Podgorski, T., Coupier, G., 2014. Pairwise hydrodynamic interactions and diffusion in a vesicle suspension. Phys. Fluids 26 (1), 013304.

Grandmaison, N., Brancherie, D., Salsac, A.-V., 2021. Modelling of damage of a liquid-core microcapsule in simple shear flow until rupture. J. Fluid Mech. 914, A25.

Guazzelli, A., Morris, J. F., 2012. A Physical Introduction to Suspension Dynamics. Cambridge University Press.

Hu, X.-Q., Lei, X.-C., Salsac, A.-V., Barthès-Biesel, 2020. Minuet motion of a pair of capsules interacting in simple shear flow. J. Fluid Mech. 892, A19.

Kachanov, L., 1986. Introduction to Continuum Damage Mechanics. Springer.

Kantsler, V., Segre, E., Steinberg, V., 2008. Dynamics of interacting vesicles and rheology of vesicle suspension in shear flow. Europh. Lett. 82 (5), 58005.

Koleva, I., Rehage, H., 2012. Deformation and orientation dynamics of polysiloxane microcapsules in linear shear flow. Soft Matter 8, 3681 – 3693.

Lac, E., Barthès-Biesel, D., 2008. Pairwise interaction of capsules in simple shear flow: Three-dimensional effects. Phys. Fluids 20 (4), 040801.

Lac, E., Barthès-Biesel, D., Pelakasis, A., Tsamopoulos, J., 2004. Spherical capsules in three–dimensional unbounded Stokes flows: effect of the membrane constitutive law and onset of buckling. J. Fluid Mech. 516, 303 – 334.

Lac, E., Morel, A., Barthès-Biesel, D., 2007. Hydrodynamic interaction between two identical capsules in a simple shear flow. J. Fluid Mech. 573, 149 – 169.

Le Goff, A., Kaoui, B., Kurzawa, G., Haszon, B., Salsac, A.-V., 2017. Squeezing biocapsules into a constriction: deformation till break-up. Soft Matter 13, 7644–7648.

Lemaitre, J., Desmorat, R., 2005. Engineering Damage Mechanics: Ductile, Creep, Fatigue and Brittle Failures. Springer.

Leopércio, B., Michelon, M., Carvalho, M., 2021. Deformation and rupture of microcapsules flowing through constricted capillary. Sci Rep 11, 7707.

Omori, T., Ishikawa, T., Imai, Y., Yamaguchi, T., 2013. Shear-induced diffusion of red blood cells in a semi-dilute suspension. J. Fluid Mech. 724, 154–174.

Pozrikidis, C. Boundary integral and singularity methods for linearized viscous flows Cambridge University Press, 1992.

Pranay, P., Anekal, S. G., Hernandez-Ortiz, J. P., Graham, M. D., 2010. Pair collisions of fluid-filled elastic capsules in shear flow: Effects of membrane properties and polymer additives. Phys. Fluids 22 (12), 123103.

Ramanujan S, Pozrikidis C. 1998. Deformation of liquid capsules enclosed by elastic membranes in simple shear flow: Large deformations and the effect of capsule viscosity. J. Fluid Mech. 361:117–143

Rehage, H., Husmann, M., Walter, A., 2002. From two–dimensional model networks to microcapsules. Rheol. Acta 41, 292.

Risso, F., Carin, M., 2004. Compression of a capsule: Mechanical laws of membranes with negligible bending stiffness. Phys. Rev. E 69, 061601 – 061608.

Singh, R. K., Sarkar, K., Dec 2015. Hydrodynamic interactions between pairs of capsules and drops in a simple shear: Effects of viscosity ratio and heterogeneous collision. Phys. Rev. E 92, 063029.

Wahlberg, B., Ghuman, H., Liu, J. R., Modo, M., 2018. Ex vivo biomechanical characterization of syringe-needle ejections for intracerebral cell delivery. Sci. Rep. 8 (1), 1–17.

Walter, A., Rehage, H., Leonhard, H., 2000. Shear–induced deformation of polyamid microcapsules. Colloid Polymer Sci. 278, 169 – 175.

Walter, J., Salsac, A.-V., Barthès-Biesel, D., Le Tallec, P., 2010. Coupling of finite element and boundary integral methods for a capsule in a Stokes flow. Int. J. Num. Meth. Engng 83, 829 – 850.

Wang, X.-Y., Merlo, A., Dupont, C., Salsac, A.-V., Barthès-Biesel, D., 2021. A microfluidic methodology to identify the mechanical properties of capsules: comparison with a microrheometric approach. Flow 1, E8.